2B.3 Modeled secondary eyewall and spiral band dynamics

Wesley D. Terwey[1] and Michael T. Montgomery
Colorado State University

I. Introduction

Secondary eyewall cycles are one of the most important, yet vexing, questions remaining in our understanding of mature hurricane structure and evolution because of the dramatic intensity changes that these cycles can have on mature hurricanes. Recent estimates put the number of storms undergoing a secondary eyewall cycle at over 50 percent of all major hurricanes (Hawkins *et al* (2004)). Our understanding of how a secondary eyewall replaces the primary eyewall is reasonably well understood (e.g. Shapiro and Willoughby, 1982), but our knowledge in how the formation of this additional eyewall feature is still in its infancy.

To investigate the secondary eyewall formation problem, we carefully examine a simplified full-physics simulation of a hurricane that underwent a clear secondary eyewall cycle. By applying dynamical diagnostics on the model fields, we begin to hypothesize potential pathways to secondary eyewall formation and the physics involved in these pathways.

II. Setup

Our initial model setup is based off of the idealized modeling work of Montgomery *et al* (2006). We are using the Regional Atmospheric Modeling System (RAMS) version 4.3.0 (Pielke *et al*. 1992, Cotton *et al*. 2003). The model is a three-dimensional, non-hydrostatic numerical model with a seven-category microphysical scheme and other physical closures and parameterizations.

Three grids are used in this simulation with horizontal spacing of 24, 6, and 2 km with overall sizes of approximately 4000, 1000, and 500 km. Thirty vertical levels are specified, stretching from the surface to approximately 26 km in height with 300 m vertical resolution near the surface to 1800 m vertical resolution near the top of the domain. Convection is explicitly simulated throughout the entire domain. The largest domain is cyclic in both horizontal directions. All layers have a sponge layer in the stratosphere. The model simulation begins with a mesoscale convective vortex (MCV) of moderate strength in a slightly moistened Jordan sounding environment with 28 degree Celsius sea surface temperature. The entire simulation is performed on an *f*-plane at 15ºN.

For future reference we will refer to this simulated storm as Hurricane Rikutsu.

III. Simulated Vortex Evolution

Figure 1 summarizes the basic evolution of Rikutsu. Minimum near-surface (lowest model grid level at 147 m) pressure is plotted in the solid line, while the dashed line shows the maximum azimuthally-averaged tangential winds.

Starting from the weak MCV, Rikutsu consolidates itself into a tropical cyclone in approximately two days, following a similar pathway as described in Montgomery *et al* (2006). Once this finishes, Rikutsu intensifies rapidly from minimal tropical storm to hurricane in about 24 hours. Through the next two days, it undergoes a period of

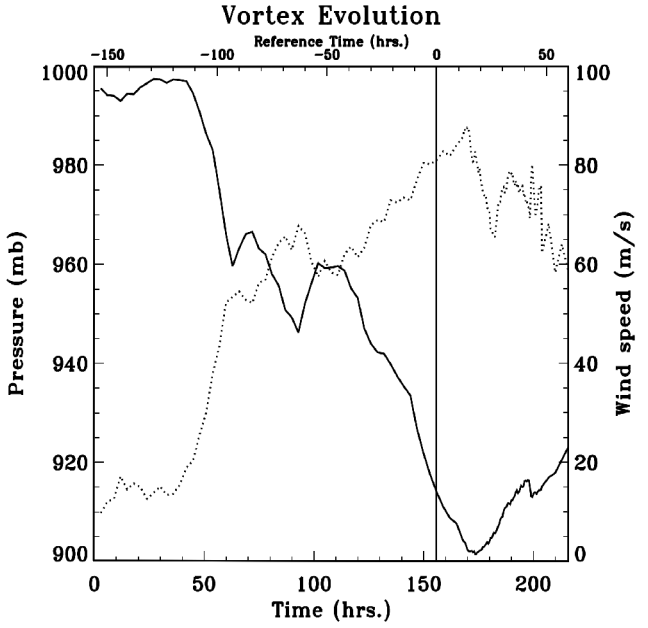

Figure 1: Evolution of the simulated Hurricane Rikutsu. Minimum near-surface pressure (solid) and maximum mean tangential winds (dotted) are shown over the time of the simulation. Three hour output is used until 168 hours into the simulation after which 30 minute output is used.

[1] *Corresponding author address: Wesley Terwey, Dept. of Atmospheric Science, Colorado State University, Fort Collins, CO 80523; email: terwey@atmos.colostate.edu*

intensity fluctuations. During this time, there is a small increasing trend in intensity as well as a gradual increasing trend in the radius of maximum winds (not shown). This is a very interesting period but will not be the subject of this report.

At about 120 hours into the simulation, Rikutsu begins a steady intensifying trend that continues for approximately two days. It is from near the end of this trend, i.e. the start of the period of maximum intensity, that we reference the time in our subsequent plots and discussion. Reference time Hour 0 is set as 156 hours into the simulation.

From Hour 0 to Hour 12, the storm strengthens slightly, the central near-surface pressure decreases to 905 mb, and azimuthally averaged winds of 85 to 90 m/s are present at the top of the boundary layer at a radius of 30 to 35 km. Shortly after this peak in winds, the near-surface pressure falls to a minimum of 902 mb. At Hour 12 the structure of Rikutsu is complex with a strong eyewall and two or three spiral bands (Figure 2). As time progresses, the inner portions of the spiral bands consolidate into two main bands. By Hour 18, the two bands have begun to grow in area and merge at their endpoints. An elliptical convective structure has formed by Hour 21 (not shown) at approximately 80 to 100 km radius. As this structure gets better organized, the inner eyewall's updrafts begin to decay appreciably, as expected by secondary eyewall replacement theory (Willoughby *et al*, 1982).

This rearrangement of Rikutsu's structure can be seen in the pressure and wind traces from Figure 1. The pressure begins rising around Hour 20, while the maximum winds have been in steady decline

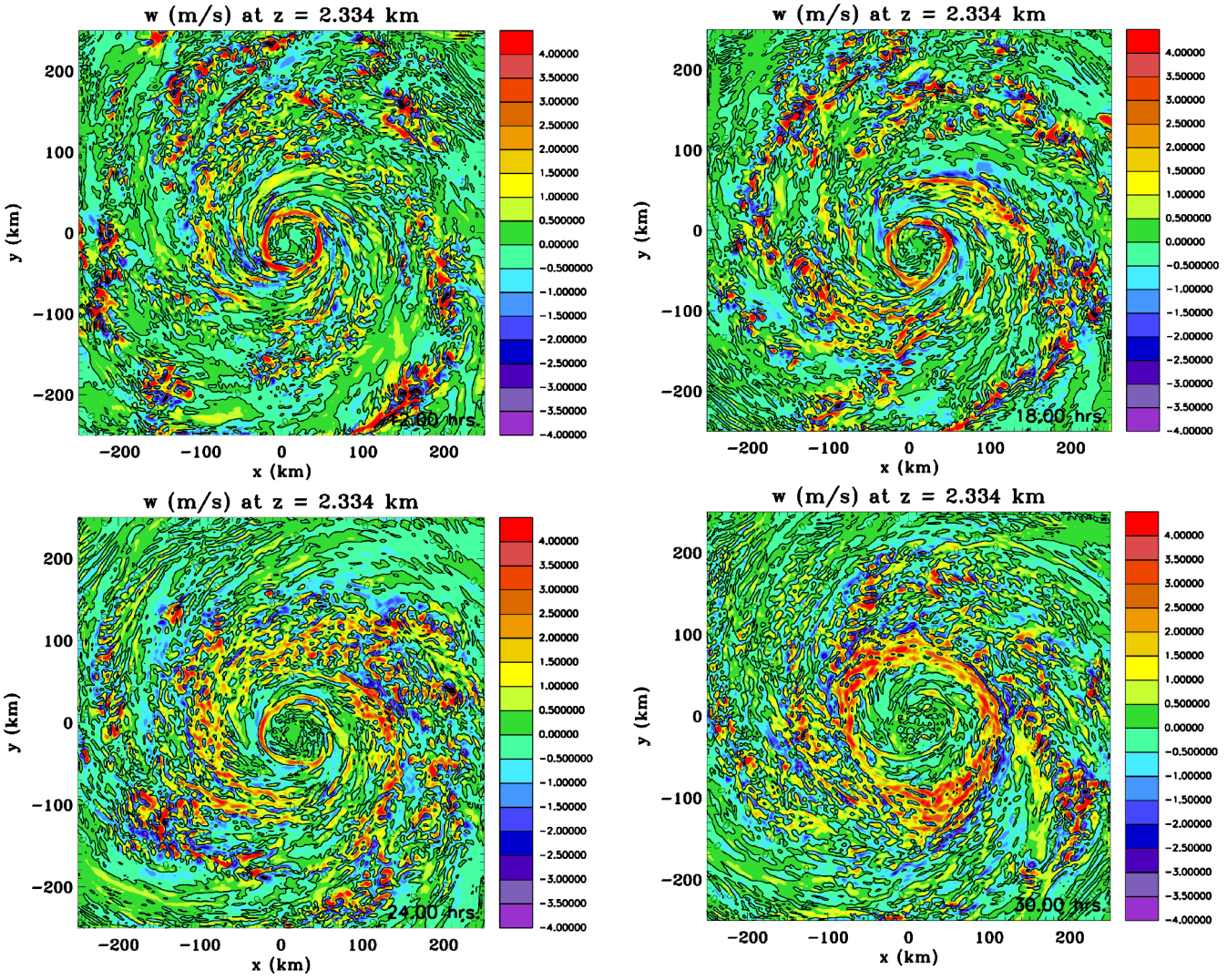

Figure 2: Four horizontal cross-sections of vertical velocity above the boundary layer. Shown are Hour 12 (top left), Hour 18 (top right), Hour 24 (bottom left), and Hour 30 (bottom right). This shows the basic evolution of the secondary eyewall in Rikutsu from the consolidation of two spiral bands into a ring-like convective structure to primary eyewall.

since the same time.

By Hour 30, Rikutsu's inner eyewall has all but disappeared and the outer one has become the dominant eyewall feature. The bands that had been prevalent outside Rikutsu's core have all but disappeared. The maximum mean winds have increased back to the 75 m/s range, but are now concentrated near the new eyewall at 80-90 km radius.

IV. Diagnosis of Cyclone Phenomena: Secondary Eyewall and Spiral Bands

In our effort to find and understand the pathways to secondary eyewall formation, we examine several diagnostic and analytical tools that may be of use with our model data. A required first step involves the examination of azimuthal mean cross-sections to get an overall idea of the mean vortex evolution. These fields show the secondary eyewall cycle very clearly.

Next, an examination of the azimuthal Fourier power spectra and decompositions of various thermodynamic and kinematic fields in the hurricane enables one to look closely at the waves inherent in the vortex. Identification of the wave types from these analyses will give us some guidance in finding the appropriate theoretical framework in which to view this problem.

An additional useful analysis is a mean tangential momentum budget. We use the one derived from Molinari *et al* (1995) in cylindrical-isentropic coordinates. Integrating their equation A4 in time, we come upon a form that can be used with our model data (Figure 3). In this equation, overbars denote azimuthal averages while primes denote perturbations from the azimuthal averages. Subscripts represent partial derivatives. u and v stand for the radial and tangential winds, respectively. σ is the pseudodensity in isentropic coordinates. $\Delta\overline{v}(T)$ is the change in the mean azimuthal velocity from time 0 to time T.

Our current secondary eyewall formation hypotheses from this analysis involve the growth of convectively-coupled waves and the forcings from their attendant secondary circulations. Expansion on the details of this hypothesis is incomplete as of this writing.

Additionally, though secondary eyewall formation is our primary research focus, a thorough examination of the spiral bands intrinsic to the formation of this particular secondary eyewall will be completed. Recent results (e.g. Chen and Yau 2003; Chen *et al*., 2003) have shown that near-core rainbands in simulated hurricanes are best approximated by vortex Rossby wave theory. However, outer rainbands, like the ones we are examining, have been discussed to potentially be a number of different waves types: vortex Rossby (e.g. Montgomery and Kallenbach, 1997), gravity (e.g. Kurihara, 1976), and "mixed" Rossby-gravity (Schecter and Montgomery, 2004). Understanding the different waveforms that comprise these bands may be a key to understanding the mechanisms of secondary eyewall formation.

V. Acknowledgments

The authors would like to acknowledge NSF grants ATM-0101781, ATM-0132006, and ATM-0528816 for their support. We would also like to thank Mel Nicholls for his assistance in setting up and running the simulation.

VI. References

Chen, Y., G. Brunet, and M. K. Yau, 2003: Spiral

$$\begin{aligned}\Delta\overline{v}(T) \;=\; & \left(\frac{\overline{\sigma}(0)}{\overline{\sigma}(T)}-1\right)\overline{v}(0)-\frac{1}{\overline{\sigma}(T)}\int_0^T\left(r^{-2}\left(r^2\left(\overline{\sigma u}\right)\overline{v}\right)_r+\left(\overline{\sigma u}\right)f\right)dt \\ & -\frac{1}{\overline{\sigma}(T)}\int_0^T\left(\left(\overline{\sigma\dot{\theta}}\right)\overline{v}\right)_\theta dt+\frac{1}{r\overline{\sigma}(T)}\int_0^T\nabla\cdot\vec{F}dt \\ & -\frac{1}{\overline{\sigma}(T)}\int_0^T\left(\overline{\left(\sigma\dot{\theta}\right)'v'}\right)_\theta dt-\frac{1}{\overline{\sigma}(T)}\left[\overline{\sigma'v'}\right]_{t=0}^T+\frac{1}{\overline{\sigma}(T)}\int_0^T\overline{\sigma F^\lambda}dt\end{aligned}$$

Figure 3: Equation A4 of Molinari et al (1995) integrated in time. This equation is the basis for our mean tangential momentum budget diagnoses to help understand the main dynamics in the mature hurricane vortex.

bands in a simulated hurricane. Part II: Wave activity diagnostics. *J. Atmos. Sci.*, **60**, 1239-1256.

Chen, Y. and M. K. Yau. 2003: Asymmetric structures in a simulated landfalling hurricane. *J. Atmos. Sci.,* **60**, 2294–2312.

Cotton, W. R. and Coauthors, 2003: RAMS 2001: Current status and future directions. *Meteorol. Atmos. Phys.*, **82**, 5-29.

Hawkins, J., and M. Helveston, 2004: Tropical cyclone multiple eyewall characteristics. Preprints, *26th Conference on Hurricanes and Tropical Meteorology*, Miami, FL, Amer. Meteor. Soc., 276-277.

Kurihara, Y., 1976: On the development of spiral bands in a tropical cyclone. *J. Atmos. Sci.*, **33**, 940-958.

Molinari, J., S. Skubis, and D. Vollaro, 1995: External influences on hurricane intensity. Part III: Potential vorticity structure. *J. Atmos. Sci.*, **52**, 3593-3606.

Montgomery, M. T., and R. J. Kallenbach, 1997: A theory for vortex Rossby-waves and its application to spiral bands and intensity changes in hurricanes. *Q. J. R. Meteorol. Soc.*, **123**, 435-465.

Montgomery, M. T., M. E. Nicholls, T. A. Cram and A. B. Saunders. 2006: A vortical hot tower route to tropical cyclogenesis. *J. Atmos. Sci.,* **63**, 355–386.

Pielke, R. A., and Coauthors, 1992: A comprehensive meteorological modeling system – RAMS. *Meteorol. Atmos. Phys.*, **49**, 69-91.

Schecter, D. A., and M. T. Montgomery, 2004: Damping and pumping of a vortex Rossby wave in a monotonic cyclone: critical layer stirring versus inertia-buoyancy wave emission. *Phys. Fluids*, **16**, 1334-1348.

Shapiro, L. J., and H. E. Willoughby, 1982: The response of balanced hurricanes to local sources of heat and momentum. *J. Atmos. Sci.*, **39**, 378-394.

Willoughby, H. E., J. A. Clos, and M. G. Shoreibah, 1982: Concentric eye walls, secondary wind maxima, and the evolution of the hurricane vortex. *J. Atmos. Sci.*, **39**, 395-411.